Ground-state phase in the three-dimensional topological Dirac semimetal Na_3Bi

Xiyue Cheng, Ronghan Li, Yan Sun, Xing-Qiu Chen,* Dianzhong Li, and Yiyi Li

Shenyang National Laboratory for Materials Science, Institute of Metal Research, Chinese Academy of Sciences, Shenyang 110016, China

(Received 4 April 2014; published 2 June 2014)

By means of the first-principles calculations, we found that the early characterized 3D topological Dirac semimetal $P6_3/mmc$-Na_3Bi is dynamically unstable at the ground state due to the presence of the large imaginary phonon frequencies around the K point. Alternatively, our calculations suggested a new ground-state phase crystalizing in a $P\bar{3}c1$ structure with buckled graphite-like Na/Bi sheets, which is both energetically and dynamically stable. Moreover, the calculations also uncovered that the $P\bar{3}c1$ phase is a 3D topological Dirac semimetal, with exactly the same electronic states of the metastable $P6_3/mmc$ phase.

DOI: 10.1103/PhysRevB.89.245201 PACS number(s): 73.20.−r, 71.20.−b, 73.43.−f

I. INTRODUCTION

The 3D topological bulk Dirac semimetal (TDS), as a new class of topological electronic state, is highlighting an exciting frontier of the Dirac electrons. In the TDSs, the conduction and valence bands touch only at the discrete Dirac points and disperse linearly in all directions in the Brillouin zone (BZ). This electronic state is different from the 2D Dirac fermions in the graphene and the surface state of the 3D topological insulators [1–4]. The TDSs exhibit many attractive phenomena, on the one hand, in analog of graphene [5], such as the high electron mobility and conductivity in the 3D form, and on the other hand, with numerous fascinating quantum properties, including the unique surface states in form of the Fermi arcs, the Weyl phases, the high-temperature linear quantum magnetoresistance, and the topological magnetic phases as well as the quantum anomalous Hall effect [1–4,6–15]. In general, the TDSs are predicted to exist at the critical phase transition point from a normal insulator to a topological one through the spin-orbit coupling effect or by tuning the chemical composition [9,16]. However, such bulk Dirac points are accidental degeneracies. Interestingly, very recently the systems of the $P6_3/mmc$-Na_3Bi [1–3], Cd_3As_2 [10,17,18], and β-BiO_2 [4] have been theoretically predicted to be the TDSs in their native phases and the former two compounds were even experimentally demonstrated as their 3D bulk Dirac fermions are indeed protected by the crystallographic symmetry.

In particular, it has been reported that the crystal structure of the 3D topological bulk Dirac semimetal Na_3Bi adopts the Na_3As-type structure [1–3] with the space group of $P6_3/mmc$ and $Z = 2$, which was firstly derived in 1937 by Brauer and Zintl [19] from a Deby-Scherrer pattern, as shown in Fig. 1(a). However, as a matter of fact, the structure of the prototype compound Na_3As was reinvestigated to other two closely correlated ones: the $P\bar{3}c1$ [anti-LaF_3-type, $Z = 6$, Fig. 1(d)] and the $P6_3cm$ [Cu_3P-type, $Z = 6$, Fig. 1(g)], which were revealed by Mansmann [20] and Hafner *et al.* [21,22], respectively. Interestingly, because these two structures are so close to each other that their x-ray diffraction (XRD) patterns are almost indistinguishable for a specified compound [23,24]. In most experimental characterizations, the $P6_3cm$-type structure is favored in the alkali-metal pnictides or nitrides or some intermetallic phases [25–27], such as K_3Bi [28], Cs_3As [29], Mg_3Pt, and Mg_3Cu [23], while the $P\bar{3}c1$ phase is preferred in the trifluorides of the lanthanum group elements [24]. However, according to the Pearson's Handbook [30], Na_3Bi was attributed to the earlier characterized $P6_3/mmc$ structure and the later studies focusing on Na_3Bi [1,2,31–38] all follow this structure. Because of these historical uncertainties on its structure, it is an urgent task to clarify the ground-state phase of Na_3Bi.

Here, by means of the first-principles calculations, we have systematically investigated the phase stabilities and the electronic structures of Na_3Bi at the ground state. Our calculated results uncovered that the $P\bar{3}c1$ structure is the energetically favorable ground-state phase with thermodynamic and dynamic stabilities. However, the early characterized $P6_3/mmc$ structure was found dynamically unstable with several large imaginary transverse acoustic (TA) modes around the high-symmetry K point. Importantly, their electronic band structures are similar to each other, featured by two 3D bulk Dirac fermions protected by the threefold rotated crystal symmetry. Therefore, our calculated results suggest that the ground-state $P\bar{3}c1$ phase of Na_3Bi is also a robust TDS.

II. COMPUTATIONAL METHOD

The structural optimization and the electronic properties of the Na_3Bi phases were calculated within the framework of density functional theory (DFT) [39,40] by employing the Vienna *ab initio* simulation package (VASP) [41,42]. The projector augmented wave (PAW) method [43] and the generalized gradient approximation (GGA) within the Perdew-Burke-Ernzerhof (PBE) exchange-correlation functional [44] were applied. The adopted PAW-PBE pseudopotentials of Na and Bi treat $2p^6 3s^1$ and $5d^{10} 6s^2 6p^3$ electrons as valences, respectively. The energy cutoff was set at 350 eV and the appropriate Monkhorst-Pack k meshes were chosen. A very accurate optimization of structural parameters was achieved by minimizing forces (below 0.0001 eV/Å) and stress tensors (typically below 0.5 k_B). To check the dynamical stability, we further derived the phonon dispersion curves using the finite-displacement approach as implemented in the *Phonopy* code [45]. The phonon frequency are constructed from forces, resulting from displacements of certain atoms in a supercell containing $3 \times 3 \times 3$, $2 \times 2 \times 2$, and $2 \times 2 \times 2$ unit cells for

*Corresponding author: xingqiu.chen@imr.ac.cn

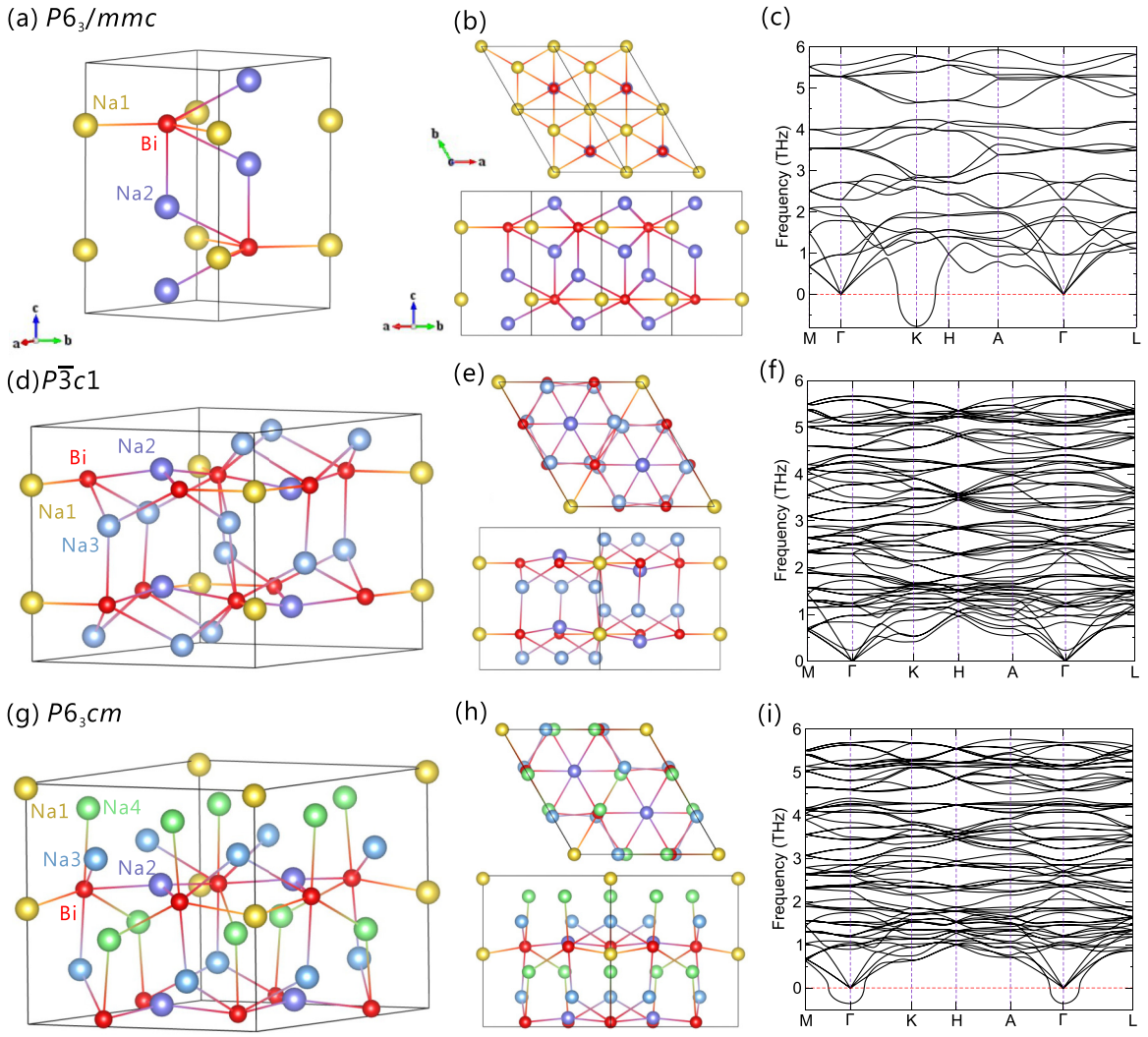

FIG. 1. (Color online) The structure representations of (a) the original $P6_3/mmc$ (Na_3As-type) structure, (d) the $P\bar{3}c1$ (anti-LaF_3-type), and (g) the $P6_3cm$ (Cu_3P-type) structures of Na_3Bi. The projections along the [0001] and [11$\bar{2}$0] directions for these three structures are shown in (b, e, and h), together with the phonon dispersion curves in (c, f, and i), respectively. Note that a $2 \times 2 \times 1$ supercell for the $P6_3/mmc$-Na_3Bi is used in the projection image (b). It needs to be emphasized that for these three structures, the Bi atoms share the exactly same network, while the Na atoms are highly distort. As listed in Table I, the $P6_3/mmc$, $P\bar{3}c1$, and $P6_3cm$ structure hold two, three, and four inequivalent Na atoms, respectively.

the $P6_3/mmc$, $P\bar{3}c1$, and $P6_3cm$ structures, respectively. To calculate the surface electronic band structures of the $P\bar{3}c1$ phase, we have constructed the tight-binding (TB) model Hamilton according to the DFT band structure with the SOC inclusion. The TB matrix elements are calculated by projecting onto the maximally localized Wannier orbitals [46–48], using the VASP2WANNIER90 interface [49]. Utilizing these bulk TB Hamilton matrix elements, we have built the slab models of the (0001) and (01$\bar{1}$0) surfaces and derived the surface electronic band states.

III. RESULTS AND DISCUSSIONS

The relative stabilities of the three structures ($P6_3/mmc$, $P\bar{3}c1$, and $P6_3cm$) considered here for Na_3Bi can be visualized from the energy-versus-volume curves in Fig. 2. The $P\bar{3}c1$ phase is about 4 meV/f.u. lower in energy than the $P6_3/mmc$ structure. This small energy difference suggests that the metastable $P6_3/mmc$ structure can be stable at low temperature. Given the simple relation [50] of $\Delta E = k_B T$, it is further estimated that the phase transition temperature is about 46 K. Interestingly, the volume-dependent energies of the $P6_3cm$ structure are comparable to the $P\bar{3}c1$ one in Fig. 2. Their optimized lattice parameters are further compiled in Table I as compared with available experimental findings. Note that, as early as 1965, Mansmann [20] suspected that Na_3Bi crystalizes in the $P\bar{3}c1$ structure and refined its lattice constants, which are in good agreement with our currently derived data in Table I.

From Table I, it can be seen that the $P6_3/mmc$ phase has two formula units per unit cell ($Z = 2$), which is about one-third the size of the other two competing structures ($Z = 6$). For the $P6_3/mmc$ phase, the Bi atom lies at the $2c$ site (1/3, 2/3, 1/4) and the Na atoms occupy other two inequivalent sites, Na1 at $2b$ site (0, 0, 1/4), and Na2 at $4f$ site (1/3, 2/3, 0.5827). This situation leads to a layered structure with the stacking sequence

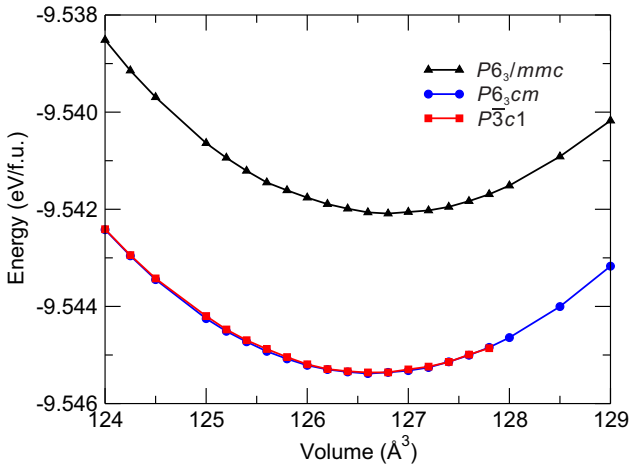

FIG. 2. (Color online) The energy-versus-volume curves for the $P6_3/mmc$, $P6_3cm$, and $P\bar{3}c1$ structures of Na_3Bi.

of Na-(graphite-like Na/Bi sheet)-Na and these graphite-like Na/Bi sheets are separated by the sodium atoms, as illustrated in Figs. 1(a) and 1(b). The Na-Bi distances within the graphite-like layers are around 3.151 Å and the vertical Na-Bi bonds between the adjacent layers are about 3.228 Å ; thus, the Na and Bi atoms form a base-centered tetrahedron.

In fact, the $P\bar{3}c1$ structure is closely correlated with the $P6_3/mmc$ one. However, the important difference is that the layered graphite-like Na/Bi sheets are distorted [Figs. 1(d) and 1(e)] in the $P\bar{3}c1$ phase. First, partial Na1 atoms in the $P6_3/mmc$ phase along the c axis shift up or down about 0.05 Å leading to the buckled graphite-like Na/Bi sheets in the $P\bar{3}c1$ structure. Second, the original Na2 atoms in the $P6_3/mmc$ phase distort within the ab plane. Therefore, there are three inequivalent Na Wykoff sites in the $P\bar{3}c1$ structure [see Table I and Fig. 1(d)]. Meanwhile, the Bi atom is surrounded by seven

TABLE I. The calculated equilibrium lattice constants of a (Å) and c (Å), the difference in total energy ΔE (meV/f.u.), and the optimized atomic sites for the $P6_3/mmc$, $P\bar{3}c1$, and $P6_3cm$ phases of Na_3Bi.

				Atomic sites			
	a	c	ΔE	Atom	x	y	z
$P6_3/mmc$	5.458	9.704	4.074	Na1	0	0	0.25
	5.448[a]	9.655[a]		Na2	0.3333	0.6667	0.5827
	5.459[b]	9.674[b]		Bi	0.3333	0.6667	0.25
$P\bar{3}c1$	9.459	9.674	0	Na1	0	0	0.25
	9.436[c]	9.655[c]		Na2	0.3333	0.6667	0.2003
				Na3	0.3542	0.3187	0.0833
				Bi	0.3368	0	0.25
$P6_3cm$	9.456	9.678	0.026	Na1	0	0	0.9809
				Na2	0.3333	0.6667	0.0582
				Na3	0.6970	0	0.1972
				Na4	0.3585	0	0.3637
				Bi	0.3309	0	0.0303

[a]Reference [2].
[b]Reference [19].
[c]Reference [20].

Na atoms and the Na-Bi interacting distances range from 3.176 to 3.495 Å in the $P\bar{3}c1$ phase, which are slightly larger than those in the $P6_3/mmc$ structure.

Moreover, the $P6_3cm$ structure share a similar feature of this $P\bar{3}c1$ phase with the buckled graphite-like Na/Bi sheets. Nevertheless, their differences are also highly obvious. In the $P\bar{3}c1$ structure, the Na1 and Bi atoms lie in the same layer and the Na2 atoms are out of the plane comprised by Na1 and Bi. However, in the $P6_3cm$ structure, the Na1 atom does not lie in the same layer of Bi atoms. This difference can be clearly visualized from their projections along both [0001] and [11$\bar{2}$0] directions [Figs. 1(e) and 1(h)]. It needs to be emphasized that K_3Bi was experimentally suggested to crystallize in this $P6_3cm$ structure [28]. A complete description of that structure can be referred to Olofsson's detailed discussion [27].

From Figs. 1(c) and 1(i), the $P6_3/mmc$ and $P6_3cm$ phases exhibit imaginary phonon frequencies around the K and Γ point, respectively. These facts demonstrate their structural dynamic instabilities at the ground state. For the $P6_3/mmc$ structure, from the analysis of the eigenvectors we found two soft transverse acoustic (TA) modes on Na atoms being orthogonal to the bismuth plane. It reveals that the $P6_3/mmc$ phase can be converted into a dynamically stable structure by tuning the Na atoms along the direction of soft modes. Fortunately, these atomic vibrational directions are the same as the orientations that the Na atoms distort to in the $P\bar{3}c1$ structure, as discussed above [Figs. 1(b) and 1(e)]. As a further supporting evidence, there are no imaginary phonon frequencies in the $P\bar{3}c1$ structure [Fig. 1(f)], indicating its dynamic stability at the ground state. For the $P6_3cm$ phase, although it is energetically comparable with the $P\bar{3}c1$ one, the soft TA modes around the Γ point show its nature of dynamical instability. Therefore, among these three structures, the $P\bar{3}c1$ phase is the only one with both the lowest energy and the dynamic stability at the ground state.

Because the valence electron number of Na is much less than that of Bi and the Bi networks remain unchanged in these three structures, it is highly difficult to distinct them from the powder XRD patterns. For the $P\bar{3}c1$ and $P6_3cm$ structures, as analyzed in detail for the system of LaF_3 and Na_3N [23,24], the XRD patterns for both structures are so close to each other that it is impossible to distinguish them. Luckily, through our calculations for Na_3Bi, the candidate of the $P6_3cm$ structure can be safely excluded due to its instability of phonon dispersion at the ground state [Fig. 1(i)]. On the other hand, we note that the simulated XRD patterns (Cu K_α, Fig. 3) for the metastable $P6_3/mmc$ structure and the ground-state $P\bar{3}c1$ one show minor differences. As illustrated in Fig. 3, it is clear that there are two additional small peaks at both (022) and ($\bar{1}$31) planes in the $P\bar{3}c1$ phase. Therefore, we believe that the careful XRD experimental measurements can effectively distinguish these two phases.

Figure 4 compiles the calculated electronic structure of the $P\bar{3}c1$ phase. It has been noted that the electronic structures are almost the same with what the metastable $P6_3/mmc$ structure exhibits [1]. From the density of states in Fig. 4(a), the Na-3s and Bi-6p states dominate the valence and conduction bands, respectively. As evidenced in Fig. 4(b), the top valence bands are mostly occupied by the Bi-6$p_{x,y}$ states, whereas the conduction bands are mainly comprised by the Na-3s states

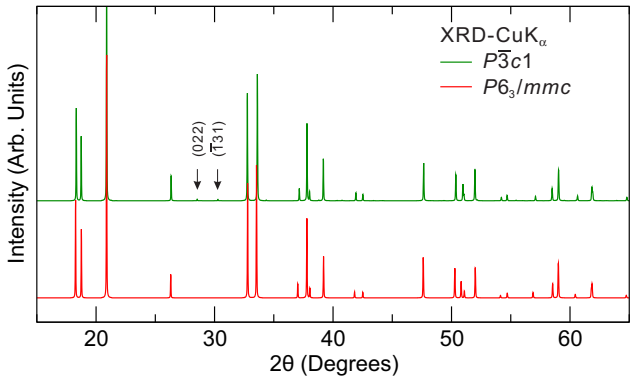

FIG. 3. (Color online) The simulated XRD patterns, using Cu K_α radiation with $\lambda = 1.5444$ Å for the $P\bar{3}c1$ (green) and $P6_3/mmc$ (red) structures.

with highly strong dispersion. Similar to the $P6_3/mmc$ phase, the $P\bar{3}c1$ structure also shows an inverted band structure, which becomes its most crucial feature. In the case without the inclusion of the spin-orbit coupling (SOC) effect, the Na-3s state lies in the valence bands, being energetically lower than the Bi-6$p_{x,y}$ states by about 0.26 eV at the Γ point. By switching on the SOC effect, the Na-3s state becomes even lower in energy by 0.75 eV than the Bi-6$p_{x,y}$ states.

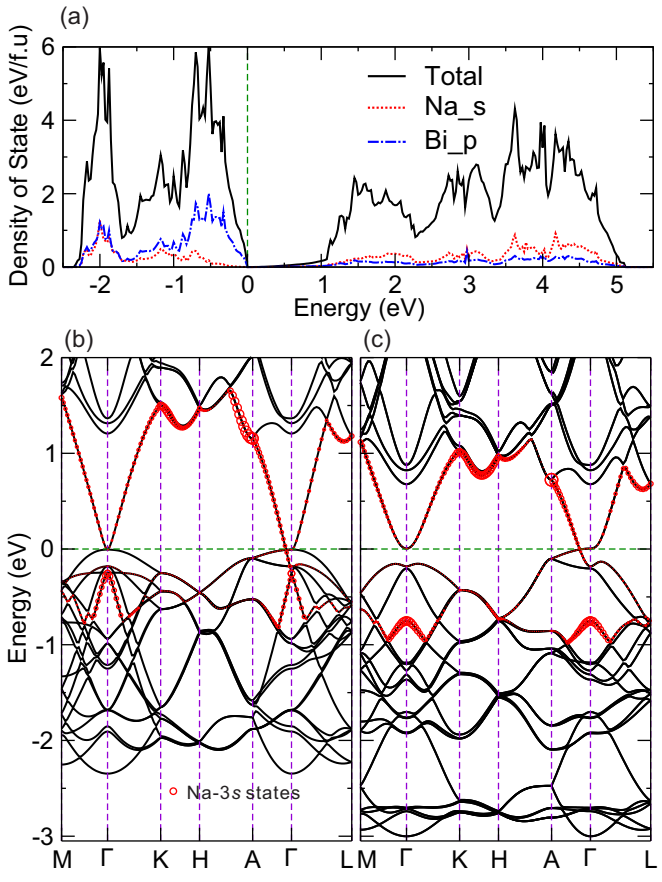

FIG. 4. (Color online) The calculated electronic structures of the $P\bar{3}c1$-Na_3Bi. (a) The total and partial density of states. (b) and (c) The band structures without and with the spin-orbit-coupling effects, respectively. The red circles indicate the projection to the Na-3s states.

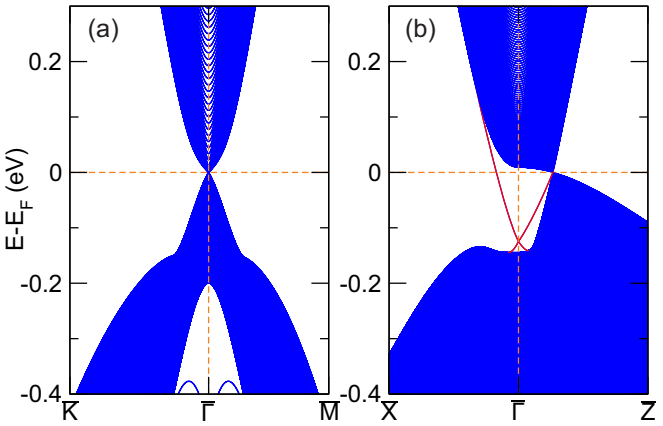

FIG. 5. (Color online) The derived surface electronic band structures of the $P\bar{3}c1$ phase of Na_3Bi: (a) the (0001) surface and (b) the (01$\bar{1}$0) surfaces.

Although the inverted band structure appears, the $P\bar{3}c1$ phase is not a nontrivial topological insulator. In contrast, it is also a topological semimetal with two 3D bulk Dirac points at (0, 0, $k_z \approx \pm 0.256\frac{\pi}{c}$) along the Γ-A direction, as shown in Fig. 4(c), being exactly the same with those of the $P6_3/mmc$ phase. Importantly, these 3D Dirac cones are protected by the threefold rotated crystal symmetry in the $P\bar{3}c1$ structure. Although in this case the graphite-like Na/Bi sheets are buckled due to the shifting of Na atoms, its threefold rotated symmetry remains unchanged. Within this condition, the 3D bulk Dirac cones would be highly robust. In addition, it needs to be mentioned that each 3D bulk Dirac cone is fourfold degenerated, linearly dispersing around the Fermi point. The appearance of these 3D bulk Dirac cones can be viewed as the "3D graphene" [1,2].

As what has been calculated for the $P6_3/mmc$ phase [1,2], we have also calculated the surface electronic bands of the $P\bar{3}c1$-Na_3Bi using the *ab initio* TB model, as presented in Fig. 5. The *ab initio* TB model is constructed by downfolding the bulk energy bands, obtained by the first-principles calculations, through the maximally localized Wannier functions (MLWFs). The surface band structures are obtained by adopting two slabs for the (0001) and (01$\bar{1}$0) surfaces with 100 and 300 unit cells, respectively. Basically, it can been seen that the surface electronic states for both the (0001) and (01$\bar{1}$0) surfaces considered here are very similar to those of the $P6_3/mmc$ phase [1,2], since the $P\bar{3}c1$ phase preserves the inverted band ordering at Γ and the threefold rotated symmetry around the c axis. From Fig. 5(a), there appears only one Dirac cone for the (0001) surface. In particular, the surface and bulk states cannot be distinguished at this cone since the Γ-A direction in the bulk 3D BZ is projected to only one point, $\bar{\Gamma}$, in the 2D BZ on the (0001) surface. In contrast, as illustrated in Fig. 5(b) our calculated electronic band structures of the (01$\bar{1}$0) surface exhibit two Dirac cones. The Dirac cone at $\bar{\Gamma}$ is twofold degenerated due to the time reversal symmetry and the Z_2 topological band inversion at Γ in its 3D BZ, whereas another Dirac cone along the $\bar{\Gamma}$-$\bar{Z}$ direction is fourfold degenerated, which is originated from the projection of the bulk 3D Dirac cone.

IV. CONCLUSION

Summarizing, in comparison with the early characterized $P6_3/mmc$ phase of Na_3Bi, we found a new ground-state phase of the $P\bar{3}c1$ structure, which is both energetically and dynamically stable. Interestingly, the $P6_3/mmc$ phase was found dynamically unstable at the ground state due to the presence of the imaginary phonon frequencies around the K point in the BZ. Meanwhile, another highly related $P6_3cm$ phase was also excluded because of its dynamical instability at ground state, although it is energetically comparable to the $P\bar{3}c1$ one. We also provided the simulated XRD pattern to distinguish the $P6_3/mmc$ and the $P\bar{3}c1$ phase. Fortunately, two additional small peaks at (022) and ($\bar{1}31$) planes of the $P\bar{3}c1$ were noticed, which are useful in the further experimental characterizations. Particularly, our calculation on the electronic structures uncovered that this ground-state $P\bar{3}c1$ phase is a topological 3D Dirac semimetal, exhibiting exactly the same electronic states as the metastable $P6_3/mmc$ phase. In addition, the *ab initio* TB model was utilized to calculate the surface states of the $P\bar{3}c1$ phase and the two characteristic Dirac cones of the TDS were clearly visualized. Noted that our present proposed ground-state $P\bar{3}c1$ phase of Na_3Bi does not present any obvious differences of the electronic structures in comparison with the metastable $P6_3/mmc$ phase [1,2].

ACKNOWLEDGMENTS

The authors are grateful for financial supports from the "Hundred Talents Project" of the Chinese Academy of Sciences (CAS) and from the National Natural Science Foundation of China (NSFC) (Grant No. 51074151). Calculations in China were performed in the HPC cluster at IMR.

[1] Z. Wang, Y. Sun, X.-Q. Chen, C. Franchini, G. Xu, H. Weng, X. Dai, and Z. Fang, Phys. Rev. B **85**, 195320 (2012).
[2] Z. K. Liu, B. Zhou, Y. Zhang, Z. J. Wang, H. M. Weng, D. Prabhakaran, S.-K. Mo, Z. X. Shen, Z. Fang, X. Dai, Z. Hussain, and Y. L. Chen, Science **343**, 864 (2014).
[3] S.-Y. Xu, C. Liu, S. K. Kushwaha, T.-R. Chang, J. W. Krizan, R. Sankar, C. M. Polley, J. Adell, T. Balasubramanian, K. Miyamoto, N. Alidoust, G. Bian, M. Neupane, I. Belopolski, H.-T. Jeng, C.-Y. Huang, W.-F. Tsai, H. Lin, F. C. Chou, T. Okuda, A. Bansil, R. J. Cava, and M. Z. Hasan, arXiv:1312.7624 [cond-mat.mes-hall].
[4] S. M. Young, S. Zaheer, J. C. Y. Teo, C. L. Kane, E. J. Mele, and A. M. Rappe, Phys. Rev. Lett. **108**, 140405 (2012).
[5] A. H. Castro Neto, N. M. R. Peres, K. S. Novoselov, and A. K. Geim, Rev. Mod. Phys. **81**, 109 (2009).
[6] X. G. Wan, A. M. Turner, A. Vishwanath, and S. Y. Savrasov, Phys. Rev. B **83**, 205101 (2011).
[7] Z. Fang, N. Nagaosa, K. S. Takahashi, A. Asamitsu, R. Mathieu, T. Ogasawara, H. Yamada, M. Kawasaki, and K. Terakura, Science **302**, 92 (2003).
[8] G. B. Halasz and L. Balents, Phys. Rev. B **85**, 035103 (2012).
[9] S. Murakami, New J. Phys. **9**, 356 (2007).
[10] Z. Wang, H. Weng, Q. Wu, X. Dai, and Z. Fang, Phys. Rev. B **88**, 125427 (2013).
[11] K.-Y. Yang, Y.-M. Lu, and Y. Ran, Phys. Rev. B **84**, 075129 (2011).
[12] M. Orlita, D. M. Basko, M. S. Zholudev, F. Teppe, W. Knap, V. I. Gavrilenko, N. N. Mikhailov, S. A. Dvoretskii, P. Neugebauer, and C. Faugeras, Nature Phys. **10**, 233 (2014).
[13] M. N. Chernodub, A. Cortijo, A. G. Grushin, K. Landsteiner, and M. A. H. Vozmediano, Phys. Rev. B **89**, 081407(R) (2014).
[14] E. V. Gorbar, V. A. Miransky, and I. A. Shovkovy, Phys. Rev. B **89**, 085126 (2014).
[15] Y. Ominato and M. Koshino, Phys. Rev. B **89**, 054202 (2014).
[16] S. M. Young, S. Chowdhury, E. J. Walter, E. J. Mele, C. L. Kane, and A. M. Rappe, Phys. Rev. B **84**, 085106 (2011).
[17] M. Neupane, S.-Y. Xu, R. Sankar, N. Alidoust, G. Bian, C. Liu, I. Belopolski, T.-R. Chang, H.-T. Jeng, H. Lin, A. Bansil, F. Chou, and M. Z. Hasan, Nat. Commun. **5**, 3786 (2014).
[18] S. Borisenko, Q. Gibson, D. Evtushinsky, V. Zabolotnyy, B. Buechner, and R. J. Cava, arXiv:1309.7978 [cond-mat.mes-hall].
[19] G. Brauer and E. Zintl, Z. Phys. Chem. B **37**, 323 (1937).
[20] M. Mansmann, Z. Kristallogr. **122**, 399 (1965).
[21] P. Hafner and K.-J. Range, J. Alloys Comp. **216**, 7 (1994).
[22] K. J. Range, R. Ehrl, and P. Hafner, J. Alloys Comp. **240**, 19 (1996).
[23] G. V. Vajenine, X. Wang, I. Efthimiopoulos, S. Karmakar, K. Syassen, and M. Hanfland, Phys. Rev. B **79**, 224107 (2009).
[24] W. A. Crichton, P. Bouvier, B. Winkler, and A. Grzechnik, Dalton Trans. **39**, 4302 (2010).
[25] K.-J. Range and P. Hafner, J. Alloys Comp. **183**, 430 (1992).
[26] K.-J. Range and P. Hafner, J. Alloys Comp. **191**, L5 (1993).
[27] O. Olofsson, Acta Chem. Scand. **26**, 2777 (1972).
[28] H. Kerber, H.-J. Deiseroth, and R. Walther, Z. Kristallogr. New Cryst. Struct. **213**, 473 (1998).
[29] H. Hirt and H. J. Deiseroth, Z. Kristallogr. New Cryst. Struct. **218**, 6 (2003).
[30] P. Villars and L. D. Calvert, *Pearson's Handbook of Crystallographic Data for Intermetallic Phase* (American Society for Metals, Metals Park, OH, 1985).
[31] H. J. Beister, S. Haag, and R. Kniep, Angew. Chem. **100**, 1116 (1988).
[32] S. Takeda and S. Tamaki, J. Phys.: Condens. Matter. **2**, 10173 (1990).
[33] H. J. Beister, J. Klein, I. Schewe, and K. Syassen, High Press. Res. **7**, 91 (1991).
[34] J. Sangster and A. D. Pelton, J. Phase Equil. **12**, 451 (1991).
[35] M. Tegze and J. Hafner, J. Phys.: Condens. Matter **4**, 2449 (1992).
[36] M. E. Leonova, S. A. Kulinich, L. G. Sevast'yanova, O. K. Gulish, O. V. Kravchenko, K. P. Burdina, and K. N. Semenenko, Exp. Geosci. **7**, 55 (1998).
[37] S. A. Kulinich, M. E. Leonova, L. G. Sevast'yanova, O. K. Gulish, and K. P. Burdina, Zh. Obshch. Khim. **69**, 681 (1999).
[38] M. E. Leonova, I. K. Bdikin, S. A. Kulinich, O. K. Gulish, L. G. Sevast'yanova, and K. P. Burdina, Inorg. Mater. **39**, 266 (2003).

[39] P. Hohenberg, Phys. Rev. **136**, B864 (1964).
[40] W. Kohn and L. J. Sham, Phys. Rev. **140**, A1133 (1965).
[41] G. Kresse and J. Hafner, Phys. Rev. B **47**, 558 (1993).
[42] G. Kresse and J. Furthmüller, Phys. Rev. B **54**, 11169 (1996).
[43] P. E. Blöchl, Phys. Rev. B **50**, 17953 (1994).
[44] J. P. Perdew, K. Burke, and M. Ernzerhof, Phys. Rev. Lett. **77**, 3865 (1996).
[45] A. Togo, F. Oba, and I. Tanaka, Phys. Rev. B **78**, 134106 (2008).
[46] N. Marzari and D. Vanderbilt, Phys. Rev. B **56**, 12847 (1997).
[47] I. Souza, N. Marzari, and D. Vanderbilt, Phys. Rev. B **65**, 035109 (2001).
[48] A. A. Mostofi, J. R. Yates, Y. S. Lee, I. Souza, D. Vanderbilt, and N. Marzari, Comput. Phys. Commun. **178**, 685 (2008).
[49] C. Franchini, R. Kovik, M. Marsman, S. S. Murthy, J. He, C. Ederer, and G. Kresse, J. Phys.: Condens. Matter **24**, 235602 (2012).
[50] N. W. Ashcroft and N. D. Mermin, *Solid State Physics* (Harcourt, Orlando, 1976).